

https://doi.org/10.1093/pnasnexus/pgae492
Advance access publication 4 November 2024
Research Report

Molecular basis for thermogenesis and volatile production in the titan arum

Alveena Zulfiqar $\mathbb{D}^{a,b,1}$, Beenish J. Azhar $\mathbb{D}^{a,b,1}$, Samina N. Shakeel^{a,b}, William Thives Santos \mathbb{D}^c , Theresa D. Barry \mathbb{D}^a , Dana Ozimek \mathbb{D}^a , Kim DeLong^a, Ruthie Angelovici \mathbb{D}^d , Kathleen Greenham $\mathbb{D}^{a,e}$, Craig A. Schenck \mathbb{D}^c and G. Eric Schaller $\mathbb{D}^{a,*}$

Edited By C. Boyce

Abstract

The titan arum (Amorphophallus titanum), commonly known as the corpse flower, produces the largest unbranched inflorescence in the world. Its rare blooms last only a few days and are notable both for their burst of thermogenic activity and for the odor of rotting flesh by which they attract pollinators. Studies on the titan arum can therefor lend insight into the mechanisms underlying thermogenesis as well as the production of sulfur-based volatiles, about which little is known in plants. Here, we made use of transcriptome and metabolite analyses to uncover underlying mechanisms that enable thermogenesis and volatile production in the titan arum. The ability to perform thermogenesis correlated with the expression of genes involved in bypass steps for the mitochondrial electron transport chain, in particular alternative oxidase expression, and through our analysis is placed within the context of sugar transport and metabolism. The major odorants produced by the titan arum are dimethyl disulfide and dimethyl trisulfide, and we identified pathways for sulfur transport and metabolism that culminate in the production of methionine, which our analysis identifies as the amino acid substrate for production of these odorants. Putrescine, derived from arginine, was identified as an additional and previously unrecognized component of the titan arum's odor. Levels of free methionine and putrescine were rapidly depleted during thermogenesis, consistent with roles in production of the titan arum's odor. Models for how tissues of the titan arum contribute to thermogenesis and volatile production are proposed.

Keywords: flowering, thermogenesis, sulfur metabolism, amino acid metabolism, putrescine

Significance Statement

Thermogenesis is most associated with animals, but some plant species have also evolved the ability to produce heat. The best known of these plants is the titan arum, commonly known as the corpse flower, which produces the largest unbranched inflorescence in the world and emits the odor of rotting flesh to attract pollinators. Despite its renown, the rarity of titan arum blooms has hindered scientific analysis. Here, through use of transcriptome and metabolite analyses, we uncover fundamental information about how living organisms produce heat, how plants mimic animal characteristics of temperature and odor to facilitate pollination, and how tissue specialization facilitates these abilities.

Introduction

Thermogenesis is common to many animal species, but rare in plants, the arum family Araceae being a notable exception (1). The titan arum, Amorphophallus titanum, produces the largest unbranched inflorescence in the world, its inflorescence reaching heights of up to 3 m (2). Flowering, however, is a rare event and typically occurs about once every 5 to 7 years, with the inflorescence only lasting a few days before collapsing. The inflorescence

has a large conical spadix, consisting of the appendix and rings of male and female flowers at its base, surrounded by a spathe sheath. The titan arum is thermogenic; the temperature of the appendix rises during flowering, its heat production proposed to volatilize and assist in the distribution of the floral odorants to attract pollinators. The titan arum is commonly referred to as the corpse flower, because the mixture of odorants it produces evokes the smell of rotting flesh, the native pollinators for the titan arum



Competing Interest: The authors declare no competing interests. Received: September 27, 2024. Accepted: October 21, 2024

© The Author(s) 2024. Published by Oxford University Press on behalf of National Academy of Sciences. This is an Open Access article distributed under the terms of the Creative Commons Attribution-NonCommercial License (https://creativecommons.org/licenses/by-nc/4.0/), which permits non-commercial re-use, distribution, and reproduction in any medium, provided the original work is properly cited. For commercial re-use, please contact reprints@oup.com for reprints and translation rights for reprints. All other permissions can be obtained through our RightsLink service via the Permissions link on the article page on our site—for further information please contact journals.permissions@oup.com.

^aDepartment of Biological Sciences, Dartmouth College, Hanover, NH 03755, USA

^bDepartment of Biochemistry, Quaid-i-azam University, Islamabad 45320, Pakistan

^cDivision of Biochemistry and Interdisciplinary Plant Group, University of Missouri, Columbia, MO 65211, USA

^dDivision of Biological Sciences and Interdisciplinary Plant Group, University of Missouri, Columbia, MO 65211, USA

^eDepartment of Plant and Microbial Biology, University of Minnesota, St. Paul, MN 55108, USA

^{*}To whom correspondence should be addressed: Email: george.e.schaller@dartmouth.edu

¹Present address: Department of Plant and Microbial Biology, University of Minnesota, St. Paul, MN 55108, USA.

being carrion beetles and flies (2). Analysis of the rare blooms of the titan arum can therefore enhance our understanding of thermogenesis and volatile production.

Thermogenesis involves the transformation of chemical energy into heat and typically requires mitochondrial-associated proteins that bypass the steps of oxidative phosphorylation (3–5). When the energy for oxidative phosphorylation is diverted from the formation of ATP, it is released as heat. In animals, nonshivering thermogenesis takes place in brown adipose tissue and is reliant upon expression of uncoupling proteins (UCPs) (3). UCPs dissipate the proton gradient across the inner mitochondrial membrane such that it is not available to the ATP synthase (6). In plants, the primary focus of thermogenesis studies has been on alternative oxidases (AOXs), which divert electrons from the electron transport chain (ETC) to decrease the efficiency of oxidative phosphorylation (4). Increased levels of AOX activity correlate with thermogenesis in the arum family, studies in Sauromatum guttatum Schott (voodoo lily) indicating that salicylic acid (SA) serves as the signal for induction of thermogenesis in its appendix (4, 7-10). Although mitochondrial mechanisms for thermogenesis have been elucidated, little is known about how thermogenesis is integrated with metabolism spatially and temporally in organisms.

Plants produce an astonishing array of specialized metabolites, and many, such as floral volatile organic compounds (VOCs), exhibit spatial and temporal regulation for their biosynthesis (11, 12). A key role for floral VOCs is to attract pollinators, the specific blend of VOCs having evolved to meet the ecological niche of both flower and pollinator. Members of the Araceae family emit sweet or foul VOCs, dependent on the pollinators, those emitting foul odors doing so to attract necrophagous, saprophagous, and coprophagous insects (12-14). The composition of the VOCs is often temporally regulated, such that different odors are detected depending on the stage of flowering (15, 16). Consistent with foul odors often being derived from sulfur-based compounds, the predominant VOCs composing the carrion odor of the titan arum are dimethyl disulfide (DMDS) and dimethyl trisulfide (DMTS) (14-17). Although biosynthetic pathways for some floral VOCs have been elucidated, including various terpenoids, phenylpropanoids/benzenoids, and fatty acid derivatives, little is known about the biosynthetic pathways for production of plant sulfur-containing VOCs (10-12, 18).

Here, we took advantage of several blooms of the titan arum and employed transcriptome and metabolite analyses to address the questions of (i) what are the molecular players that mediate thermogenesis, (ii) what are the molecular players that mediate the production of VOCs, and (iii) how these are integrated spatially and temporally with plant metabolism and the transport of sugars and sulfur-based compounds. Our results reveal key pathways involved in transport and metabolism of sugars to support thermogenesis. Our results also reveal key pathways involved in production of the sulfur-based VOCs, with methionine as the amino acid substrate for their production. Additionally, we identify putrescine, derived from arginine, as a previously unrecognized component of the titan arum's odor.

Results and discussion

Transcriptome analysis of the titan arum

Only limited transcriptome information is available for thermogenic plants (10, 18, 19), and none for the titan arum. We took advantage of a 2016 bloom of the titan arum "Morphy," to collect tissue samples from the appendix, the spathe margin, and the spathe base (Fig. 1).

The appendix was chosen due to its role in thermogenesis and the production of the sulfur-based VOCs. The spathe is a bract (modified leaf) that is greenish on the outside and purplish on the inside, the purple coloration thought to play a role in the mimicry of carrion. Because the spathe is a modified leaf, we considered it likely to take on much of the normal functions of a leaf for the inflorescence. The spathe is thin at its margin and thickens at its base, indicating a potential for differing roles for these regions of the spathe. Samples were collected over three nights initiated at the night of maximal thermogenesis (day 0), commonly referred to as D-day (Fig. 1, SI Appendix Fig. S1). Temperature and odor quality were recorded for the titan arum on D-day, the outer surface of the appendix reaching a temperature ~11 °C above that of the ambient room temperature (Fig. 1, SI Appendix Fig. S1). Thermogenesis and odor quality (e.g. dead mouse, rotting fish) are consistent with reports for other titan arum blooms (2, 15). We also isolated tissue from two leaf samples, one being from a clonal plantlet derived from Morphy ("Morphy Jr.") and the second from Morphy itself when it put up a leaf in 2017. Eleven samples were isolated in total.

The nuclear genome size of the titan arum was estimated by flow cytometry using leaf tissue samples from the clonal plantlet. The 2C nuclear DNA content was estimated to be 14.04 pg (SD = 0.202), suggesting a genome size of 6,866 Mbp (1C) based on 1 pg of DNA corresponding to 978 Mbp (20). Based on an Arabidopsis (At) flow cytometry control, the titan arum genome is ~39 times the size of that found in the model plant At. No evidence for endopolyploidy of the titan arum was found by the flow cytometry analysis, consistent with the large genome size, because endoreduplication is hypothesized to be time-consuming and energetically costly for large genomes (21).

We performed RNA-seq analysis on the tissue samples collected from the titan arum, this serving two functions. First, it allowed us to generate a transcriptome assembly for the expressed genes across multiple tissues derived from the inflorescence and leaf. The de novo transcript assembly was performed with Trinity (22, 23), and resulted in the assembly of 915,085 transcripts that clustered as 536,644 genes, or a total transcriptome assembly of 266 Mbp based on the longest transcript per gene. Alternative transcripts of genes were often owed to cases in which introns were retained. Second, sampling from multiple tissues across several days enabled us to identify those differentially expressed genes (DEGs) that correlate most strongly with thermogenesis and volatile production (i.e. enriched in appendix on the night of maximal thermogenesis) (Fig. 1D; SI Appendix Fig. S2; Dataset S1). This dataset serves to define elements of the molecular toolbox by which the titan arum generates and transmits VOCs to attract pollinators. For example, Fig. 1D displays a cluster analysis of DEGs that exhibited at least a 4-fold difference in expression in the appendix at day 0 (D-day) compared with day 2 (P < 0.05). Based on this cluster analysis, substantial changes in gene expression occur over 2 days, 3,035 genes being expressed more highly and 2,750 genes being expressed at reduced levels in the appendix at D-day compared with day 2. Furthermore, there are both similarities and differences between the DEGs found in the appendix compared with the spathe tissues. The Trinity gene dataset was annotated based on its intersection with the annotated genomes of various plants, fungi, and bacteria (SI Appendix Fig. S3; Datasets S2 and S3). Below, we discuss annotated genes associated with thermogenesis and volatile production by the titan arum.

Molecular basis for thermogenesis

The titan arum produces a single treelike leaf most years, and this vegetative phase serves to store photosynthate and nutrients in

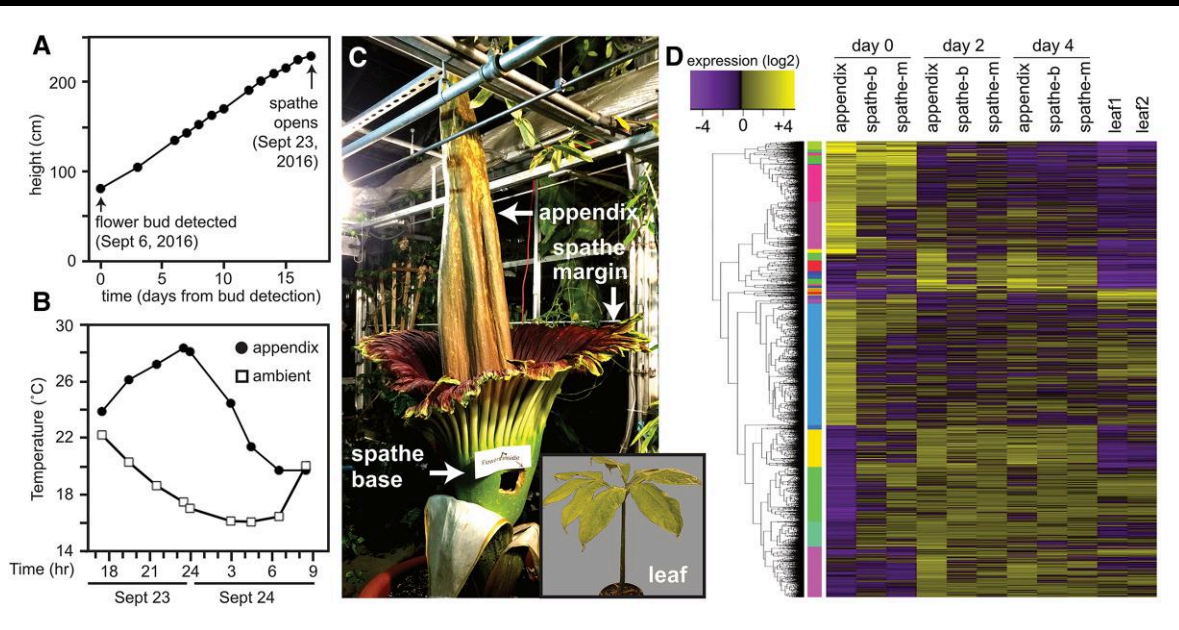


Fig. 1. Characteristics of the titan arum "Morphy" 2016 bloom. A) Growth leading up to spathe opening. Height was measured from point of soil emergence to tip of the appendix. B) Thermogenic phase of the inflorescence following opening of the spathe on 2016 September 23. The surface temperature of the appendix was measured at the same location over a period of 15 h and compared with ambient air temperature. C) Photograph of Morphy inflorescence indicating tissue types collected, and the clonal plantlet used for collection of leaf tissue ("leaf 1"; inset). D) Cluster analysis of the 5,785 DEGs that exhibited at least 4-fold expression change in appendix day 0 (D-day) compared with appendix day 2 (P < 0.05), plotted as a heatmap with dendrogram.

the underground corm tuber (24). Upon flowering, these nutrients are remobilized from the corm to the inflorescence, analysis of thermogenic arums demonstrating loss of corm biomass when flowering (24, 25). Therefore, to elucidate the molecular processes underlying thermogenesis in the titan arum, we examined the expression of genes involved in starch metabolism, sugar transport, glucose metabolism, and the bypass steps of the mitochondrial ETC associated with heat production (5, 10, 26, 27). As shown in Fig. 2A (Dataset S4), the spathe margin expresses a variety of genes associated with starch anabolism and catabolism at D-day, consistent with the spathe margin also exhibiting high expression for genes associated with photosynthesis (Dataset S4). The expression of genes involved in starch anabolism and photosynthesis by the spathe margin is similar to what is found for the leaf, and supports the spathe taking on some of the roles of a leaf during inflorescence development. In contrast, a more limited subset of genes for starch metabolism is highly expressed in the appendix; these are associated with starch catabolism, in particular beta- and alpha-amylases, consistent with the appendix having stored starch as an internal glucose reserve prior to D-day. Also consistent with the titan arum appendix making use of some internal starch reserves are ultrastructural studies on the voodoo lily (S. guttatum), in which the appendix was found to contain amyloplasts with starch granules that were depleted leading up to D-day (28). The appendix also exhibits high expression at D-day for a limited number of genes involved in sugar transport (Fig. 2A; Dataset S4), in particular for members of the STP family of plasma membrane hexose importers and for a SWEET transporter involved in facilitating diffusion of sugars to sink tissues; members of the invertase families CWI and INV are also present to cleave the disaccharide sucrose to glucose and fructose. In contrast, the spathe tissues express a broad range of genes involved in sugar transport, including those for loading sucrose into the phloem (SUT), invertases (CWI and INV), hexose transporters (STP and SWEET), and a plastid glucose transporter. Analysis of genes involved in glycolysis, the conversion of pyruvate to acetyl CoA, and the TCA cycle indicates heightened expression in the appendix at D-day (Fig. 2B; SI Appendix Fig. S4). These data support a model in which the appendix stores starch prior to D-day as an internal reserve for glucose, continues to serve as a sink tissue for sugar uptake on D-day, and has the capacity to readily mobilize and oxidize these hexoses on D-day to generate NADH.

Thermogenesis involves the transformation of chemical energy into heat and typically requires mitochondrial-associated proteins that bypass the steps by which the electrons from reduced compounds, such as NADH, are used by the ETC to power the biosynthesis of ATP (5, 10). Thermal imaging indicates that thermogenesis largely takes place in the internal cell layers of the appendix, not in the tough cuticle-covered epidermis itself, such that the appendix tissue interior is substantially hotter than its exterior (SI Appendix Fig. S5). A limited number of genes involved in cellular respiration are expressed in the appendix when compared with the spathe (Fig. 2A, Dataset S4), and these are primarily associated with bypass steps for the ETC (Fig. 2C; Dataset S4). Of particular significance, we identified genes encoding AOXs, UCPs, and alternative NAD(P)H dehydrogenases present in the titan arum transcriptome, all of which exhibited heightened expression on D-day compared with later days, with members of the AOX family exhibiting substantially higher expression in the appendix than in the spathe tissues (Fig. 2D; Dataset S4). Heightened expression and activity of AOX genes have also been correlated with thermogenesis of the appendix for the Crete arum (Arum concinnatum) and voodoo lily (9, 10) and support the model in which carbohydrates serve as the predominant respiratory substrate when AOX is employed for thermogenesis, contrasting with heightened expression of UCPs when lipids serve as the predominant respiratory substrate (29). In animals, for example, nonshivering thermogenesis takes place in brown adipose tissue and is reliant upon expression of a UCP (6). Heightened expression of genes in the titan arum associated with other

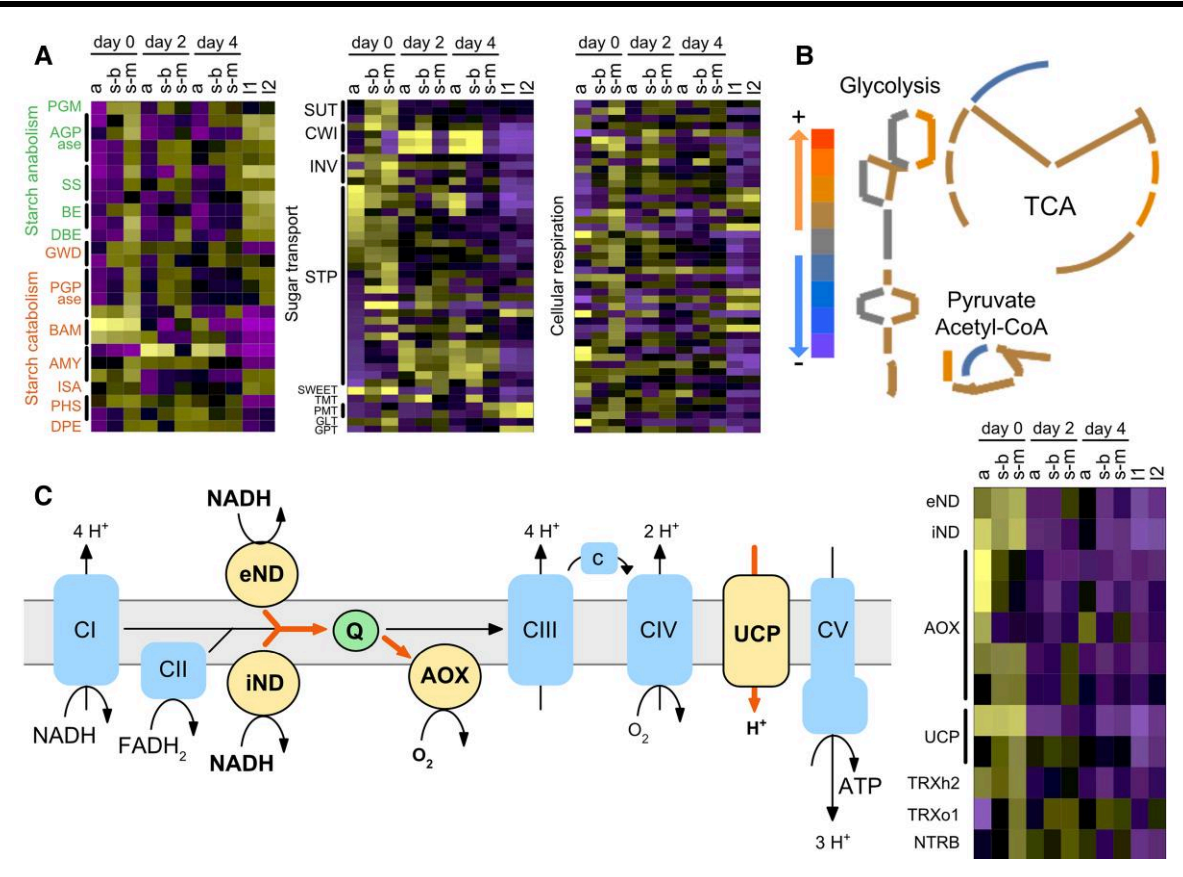


Fig. 2. Thermogenesis of the titan arum. A) Heatmaps for the expression of genes involved in starch metabolism, sugar transport, and cellular respiration (GO:0045333) in the appendix (a), spathe base (s-b), and spathe margin (s-m). Yellow, high expression; purple, low expression. B) Identification and comparative expression between days 0 and 4 of the appendix for genes involved in glucose metabolism. These are overlaid on the enzymatically catalyzed steps of glycolysis, the conversion between pyruvate and acetyl CoA, and the TCA cycle (see Fig. S4 for annotated pathways). C) Thermogenesis-related steps of the mitochondrial ETC. Shown in blue are complexes I through IV (CI–CIV) and cytochrome c of the ETC, and the ATP synthase (CV) that can be bypassed during thermogenesis. Shown in orange are the thermogenesis bypass steps, which include the external and internal alternative NAD(P)H dehydrogenases (eND and iND), AOX, and UCP. Thioredoxins (TRX) and NADPH-dependent thioredoxin reductase (NTRB) are implicated in activation of the AOX for thermogenesis. Shown in green is ubiquinone (Q), which serves as an electron carrier for both standard electron transport and thermogenesis. The heatmap shows expression of genes implicated in bypass steps for thermogenesis.

mitochondrial bypass steps of the ETC supports their contribution to thermogenesis and, based on expression in the spathe, indicates a potential capacity for the spathe to also maintain above-ambient temperatures (Fig. 2D; Dataset S4). SA is an early inducer of thermogenesis in the appendix of the voodoo lily (7, 8), and so may play a similar role in the titan arum. In the voodoo lily, the SA levels decrease prior to D-day (7, 8) and so, although we analyzed expression of genes encoding enzymes for SA metabolism in the titan arum (Dataset S4), we were not surprised these failed to correlate with thermogenesis of the appendix; such gene expression would likely be low if the titan arum followed the same developmental trajectory as the voodoo lily.

Molecular basis for production of sulfur-based volatiles

Prior analysis of the volatiles emitted by titan arums has revealed the major odorants to be the sulfur-based compounds DMDS and DMTS (14–17), VOCs that contribute to the odor of decomposing corpses (30, 31). Significantly, DMDS and DMTS were confirmed as the most abundant odorants produced by Morphy on D-day during its 2018 bloom (16). We therefore analyzed our datasets for the expression of genes associated with sulfur transport and metabolism (Fig. 3A; Dataset S4). Analysis of genes involved in sulfur transport indicates heightened expression for sulfate

transporter genes (SULTR gene family) involved in export from the vacuole and import into the chloroplast in the appendix at D-day, consistent with sulfate having accumulated in the appendix prior to thermogenesis. For sulfur metabolism in the appendix on D-day, high expression is observed for APS encoding a sulfate adenylyltransferase and APR encoding an APS reductase to convert sulfate to sulfite, along with OASTL encoding an O-acetylserine (thiol) lyase for cysteine biosynthesis. Of particular significance, CGS encoding cystathionine gamma-synthase is also highly expressed (Fig. 3A, B; Dataset S4), this enzyme serving to catalyze the first committed step in the pathway for the biosynthesis of methionine from cysteine. Thus, the appendix on D-day exhibits elevated expression of genes that will facilitate the biosynthesis of cysteine and methionine from internal sulfate stores. Analysis of genes encoding amino acid transporters (32) indicates that the appendix on D-day expresses genes for AVT amino acid transporters (Fig. 3C; Dataset S4), which serve to export amino acids from the vacuole to the cytosol, indicating that the appendix may have also stored amino acids such as methionine and cysteine to facilitate the rapid production of sulfur-containing compounds derived from these amino acids. This contrasts with the spathe tissues which express genes for a broader range of amino acid transporters.

Although the amino acids methionine and cysteine are central in the metabolism and biosynthesis of sulfur-based compounds in prokaryotes and eukaryotes, there is considerable variation in the

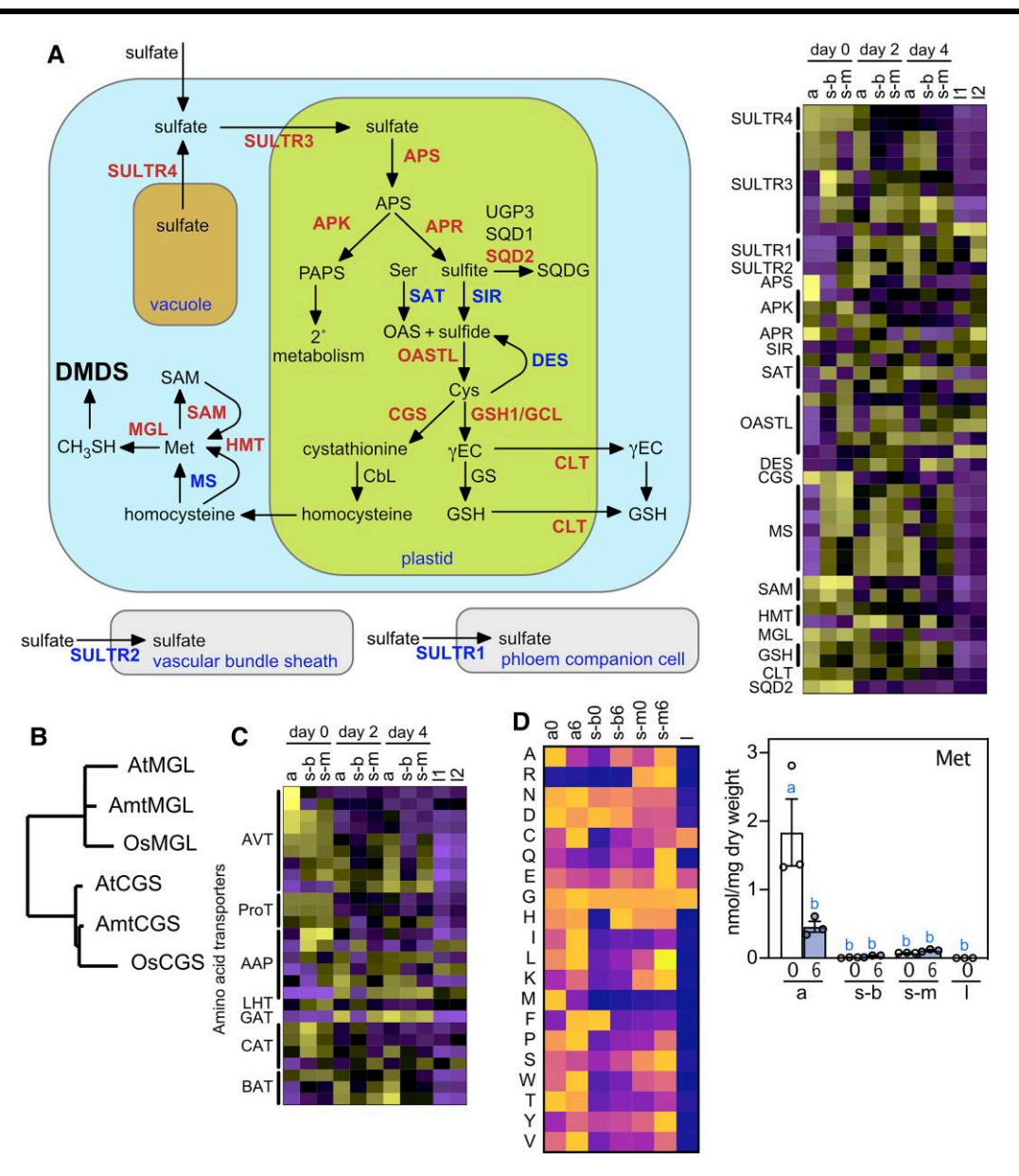


Fig. 3. Sulfur transport and metabolism of the titan arum. A) The diagram illustrates the role of key genes involved in sulfur transport (SULTR family) and sulfur metabolism, and the heatmap indicates their relative expression. On the diagram, all genes indicated in bold were identified in the titan arum; red indicates heightened expression for a family member in the appendix day 0 compared with later days, and blue indicates heightened expression for all family members in the appendix day 2 or 4 compared with day 0. B) Phylogenetic tree for CGS and MGL proteins from Arabidopsis (At), Oryza sativa (Os), and the titan arum (Amt). (C) Heatmap for the expression of genes involved in amino acid transport, including those for vacuolar exporters (AVT), proline/ glycine/GABA transporters (ProT), general amino acid permeases (AAP), lysine and histidine transporters (LHT), cationic amino acid transporters (CAT), GABA transporters (GAT), and vascular transporters (BAT). D) Free amino acid levels before (time 0 h) and after (time 6 h) peak thermogenesis of the 2022 bloom. The heatmap shows relative free amino acid concentrations; the graph shows levels of free methionine. For the graph, different blue letters indicate significant differences in methionine levels (ANOVA with post hoc Holm multiple comparison calculation, P < 0.05, n = 3).

biosynthetic and catabolic pathways proposed to produce DMDS and DMTS (33-40). We therefore analyzed the titan arum transcriptome for gene expression related to the Ehrlich and demethiolation pathways involving methionine (33-35), as well as for the alliinase and thiol S-methyltransferase pathways involving cysteine metabolism (36-40). Based on this analysis, we identified a gene encoding a methionine gamma-lyase of the demethiolation pathway that allows for the one-step production of methanethiol from methionine (Fig. 3A, B; Dataset S4) (33). Methanethiol is a common biosynthetic intermediate that, once formed, can spontaneously oxidize to DMDS and DMTS. The DEG encoding the methionine gamma-lyase was enriched at D-day in both the appendix and spathe margin, suggesting that both tissues could play a part in the production of DMDS/DMTS, with relative production likely related to the available methionine substrate and the degree of thermogenesis for the tissue.

If methionine serves as the precursor for DMDS/DMTS, methionine is predicted to be present at heightened levels in the appendix and to potentially exhibit dynamic changes in concentration during thermogenesis. We therefore took advantage of a 2022 bloom of Morphy to perform amino acid analysis on tissues harvested before and after the peak of thermogenesis (Fig. 3D, SI Appendix Fig. S5, Dataset S5). Tissue was isolated from the appendix, the spathe margin, and the spathe base, and free and

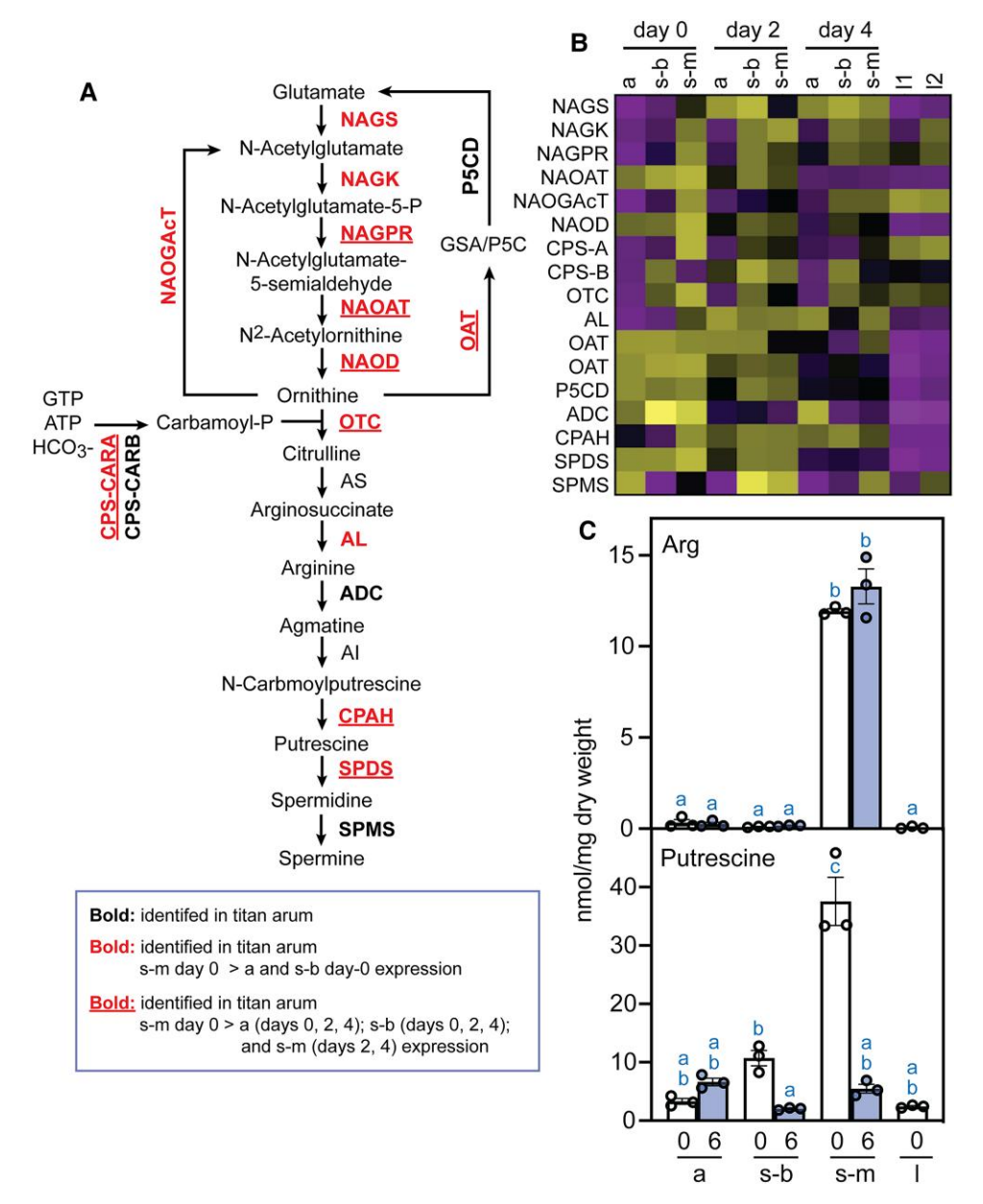


Fig. 4. Arginine and polyamine metabolism of the titan arum. A), B) Metabolic pathways and gene expression heatmap for the ornithine-dependent biosynthesis of arginine from glutamate, and the biosynthesis of the polyamines putrescine, spermidine, and spermine. On the pathway diagram, all genes indicated in bold were identified in the titan arum; red indicates heightened expression for the spathe margin (s-m) compared with the appendix and spathe base (a and s-b) on day 0; underlining indicates that maximal expression was found for the spathe margin day 0 compared with all other tissues and days. C) Levels of free arginine and putrescine before (time 0 h) and after (time 6 h) peak thermogenesis for tissues of the 2022 bloom. For the graphs, different blue letters indicate significant differences in arginine and putrescine levels (ANOVA with post hoc Holm multiple comparison calculation, P < 0.05, n = 3).

protein-bound amino acid levels were determined at the two time points, which were 6 h apart. Free methionine levels in the appendix prior to peak thermogenesis were more then 20-fold higher than in the spathe base or margin, consistent with a role as the biosynthetic precursor for DMDS/DMTS in the appendix (Fig. 3D). Furthermore, levels of free methionine were rapidly depleted over the course of thermogenesis, being reduced to 25% of the original level over the course of 6 h. No major changes were observed across tissues or times for protein-bound amino acids, indicating that these are unlikely to serve as major sources of biosynthetic precursors for odorant-based metabolites in the titan arum. Taken together, these $\,$ data are consistent with the appendix having accumulated vacuolar sulfate prior to D-day for the biosynthesis of methionine which, through the action of methionine gamma-lyase, is converted to

methanethiol and from there to DMDS/DMTS. The elevated temperature of the appendix likely facilitates the kinetics for this chemical reaction.

Identification of putrescine as an odorant derived from the spathe

Interestingly, like methionine, the free amino acid arginine also exhibited tissue-specific enrichment, but in the spathe margin rather than the appendix (Fig. 3D). Arginine serves as a biosynthetic precursor for the odorific polyamines putrescine, spermidine, and spermine (41). Putrescine is a volatile diamine that notably contributes to the rotting odor of decomposing animal flesh as the amino acids break down (30, 31). Putrescine has not previously

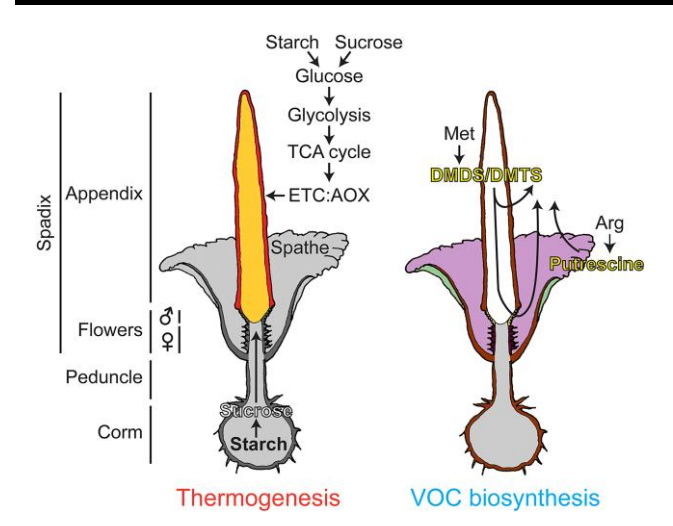


Fig. 5. Models for thermogenesis and VOC production by the titan arum. For thermogenesis, starch in the corm is transported to the appendix in the form of sucrose. In the appendix, imported sucrose and endogenous starch are converted to glucose and catabolized to produce NADH, which, through the activity of AOX in the ETC, produces heat. For VOC biosynthesis, the free amino acids Met in the appendix and Arg in the spathe are used to produce DMDS/DMTS and putrescine, respectively.

been identified as a component of the titan arum scent (13, 15) and is not readily detectable by standard gas chromatography (GC) approaches unless derivatized (42). Analysis of gene expression for enzymes involved in arginine and polyamine biosynthesis from the 2016 bloom is consistent with an enhanced ability of the spathe margin to biosynthesize arginine from the precursor glutamate and to then use arginine as the basis for polyamine biosynthesis at D-day (Fig. 4A, B). We took advantage of the 2022 bloom to determine putrescine levels pre- and post-thermogenesis in the titan arum tissues (Fig. 4C, SI Appendix Fig. S6). As shown in Fig. 4C, putrescine is 11-fold higher in the spathe margin than in the appendix and 3-fold higher than in the spathe base prior to peak thermogenesis. Additionally, levels of putrescine are rapidly depleted in the spathe over the course of thermogenesis, being reduced to ~15% of the original level in the spathe margin and base over the course of 6 h. The putrescine levels are dynamic and higher than levels found for arginine, consistent with flux through the arginine to produce putrescine and its rapid loss during thermogenesis. Thus, as with methionine to produce DMDS/ DMTS, the odorant putrescine accumulates prior to thermogenesis and is rapidly depleted during thermogenesis.

Based on our data, putrescine or one of its metabolic derivatives is likely to contribute to the odor of the titan arum. For example, putrescine can be further metabolized by a polyamine oxidase to produce 4-amino-1-butanol or by a spermidine synthase to produce spermidine (Fig. 4A). We were unable to find any matches for derivatized 4-amino-1-butanol in our samples, and potential spermidine levels could not be determined because its MS peak overlapped with those of other abundant compounds and could not be deconvoluted. That putrescine itself is the odorant is supported by the similarity of its depletion kinetics to that of methionine on D-day (Figs. 3D and 4C) and the fishy odor we and others have noted with the titan arum (SI Appendix Fig. S1) (15). The fishy odor has been attributed to the presence of trimethylamine (15), but could alternatively be due to the presence of putrescine. Of interest when considering a role for putrescine as an odorant is its production in the spathe rather than in the appendix. The spathe is a modified leaf, and as shown in Fig. 4B, the

spathe margin and titan arum leaf samples express a similar suite of genes for the biosynthetic steps leading from glutamate to citrulline. Subsequent biosynthesis of polyamines such as putrescine could take advantage of these initial biosynthetic steps.

Conclusion

Our results yield fundamental insights into the molecular mechanisms by which one of the most imposing but enigmatic members of the plant kingdom regulates thermogenesis and VOC production to attract pollinators. Dynamic changes in gene expression take place spatially and temporally during blooming of the titan arum, and this allowed us to (i) situate thermogenesis within an overall pattern of metabolism; (ii) resolve key aspects for the biosynthesis of sulfur-containing VOCs about which little is known in plants (10-12, 18); and (iii) identify putrescine as a likely component of the titan arum's odor. Our data support the models for thermogenesis and VOC production shown in Fig. 5. For thermogenesis, starch in the corm and possibly from the spathe is transported to the appendix in the form of sucrose. In the appendix, imported sucrose and endogenous starch are converted to glucose and catabolized to produce NADH, which, through the activity of AOX in the ETC, produces heat. For VOC biosynthesis, the free amino acids Met in the appendix and Arg in the spathe are used to produce DMDS/DMTS and putrescine, respectively. Although biosynthesis of DMDS/DMTS occurs in the appendix, emission is likely limited there due to the thick outer cuticle (Fig. S5E) (43), so that emission predominantly occurs instead from within the ring of male flowers. The spadix is hollow from the appendix down through the ring of male flowers (Fig. 5), so VOCs can readily circulate within this region of the spadix. This model for DMDS/DMTS emission is consistent with the observation that the predominant odor from the titan arum emanates from within the basal cup of the spathe, from where it encloses the flowers, not at the outer surface of the appendix. Furthermore, this model for emission generates a gradient of carrion odor to attract pollinators that culminates at the flowers to facilitate pollination.

Our results identify key aspects of the specialization that occurs between the appendix and spathe of the titan arum during flowering. A similar degree of specialization is likely to occur among other thermogenic arums. The spathe tissues take on much of the general metabolic burden based on their capacity for photosynthesis and starch metabolism, aerobic respiration, and the suites of sugar and amino acid transporters expressed. Specialization of the appendix is apparent in the "toolbox" associated with thermogenesis and the production of sulfur-based volatiles. Nevertheless, our data support a greater role for the spathe margin in these processes than previously recognized. In particular, the spathe margin serves as a biosynthetic source for putrescine, a likely contributor to the carrion odor of the titan arum, and has the capacity for thermogenesis based on expression of genes associated with bypass steps of the ETC. Our study also highlights the dynamic changes that take place in gene expression over just a few days during flowering of the titan arum. Of note, the appendix functions as a sink tissue on D-day but, once the utility of the appendix is served for attracting pollinators, likely shifts to a source tissue for export of its remaining nutrients based on heightened expression of genes encoding amino acid and sulfate transporters for vascular loading.

Materials and methods Plant materials

Tissues were harvested from three titan arums housed in the greenhouse of the Life Sciences Center at Dartmouth College:

"Morphy," "Morphy Junior," and "Maudine × Woody #3." For Morphy, floral tissues were harvested for transcriptome analysis from the 2016 bloom and for metabolite analysis from the 2022 bloom; leaf tissue was harvested for transcriptome analysis from the 2017 period of vegetative growth. The clonal plantlet Morphy Junior was produced by Morphy in 2016 and used for the isolation of leaf tissue for transcriptome analysis. A third titan Arum (Maudine x Woody #3; seed planted 2013 November 21) was used for collection of leaf tissue in 2022 for metabolite analysis.

Determination of DNA content

The nuclear genome size was estimated by flow cell cytometry as described (44). Three separate sections of leaf material were analyzed from the Morphy Jr. clonal plantlet, with each nuclear preparation sampled four times (i.e. three biological replicates with four technical replicates each).

Temperature measurement

Appendix temperature was measured with a Fluke 561 infrared thermometer. Ambient temperature was measured with a room sensor connected to the Argus environmental controls for the greenhouse, the sensor located ~1 m from the appendix. Thermal imaging for the 2022 bloom was performed with a Flir One Gen 3 for IOS camera.

Tissue collection for transcriptome analysis

The titan arum Morphy emerged from soil on 2016 August 18, with the flower bud detected on September 6, the spathe opening on September 23, and appendix collapse occurring six nights later. Flower tissue samples were collected from the appendix, the spathe margin, and the spathe base and flash-frozen in liquid nitrogen. Collection occurred between midnight and 1:00 AM, over three nights, each 2 days apart (days 0, 2, and 4), initiated during the night of maximal thermogenesis (D-day; day 0). Leaf tissue was collected from two sources: a leaf from the clonal plantlet Morphy Jr (leaf 1) and a leaf from Morphy that was sent up in the year that followed its flowering (leaf 2). Complete crosssections for each tissue, extending from inner to outer epidermis, were taken.

RNA isolation and library preparation

Total RNA was isolated using a modified CTAB extraction protocol for plants as described (45). The CTAB extraction buffer contained 2% (w/v) CTAB, 25 mM EDTA, 0.3 M Tris-base (pH 8.0), PVP40 3% (w/v), 2 M NaCl prewarmed to 55 °C, with 2% (v/v) β-mercaptoethanol and 50 μg/mL proteinase K added just before use. Tissue was ground to fine powder in liquid nitrogen, and then, 15 mL of CTAB buffer was used per gram tissue, and the samples were incubated at 55 °C for 15 min. Samples were extracted with 24:1 chloroform/isoamyl alcohol and then chloroform, and then, one-third volume of 8 M LiCl was added to the aqueous samples and the RNA precipitated at 4°C for 16 h. Samples were resuspended in DEPC-treated water and precipitated by the addition of one-tenth volume of 3 M NaAc and an equal volume of isopropanol, and the pellet was washed with 75% ethanol, before resuspension in DEPC-treated water.

The mRNA was isolated based on established protocols (46, 47). The mRNA fragmentation and first-strand cDNA synthesis were performed as described (46), making use of primers and reverse transcriptase for the cDNA synthesis from the YourSeq Dual FT kit (Amaryllis Nucleics). The remaining steps for cDNA synthesis and library construction were performed according to the instructions for the YourSeq Dual FT kit (Amaryllis Nucleics), with nucleic acid capture steps accomplished with AMPure XP beads (Agencourt). The concentration and quantity of the NGS libraries were determined using the DNA Qubit ds broad range kit.

Sequencing and analysis

RNA-seg was performed by BGI with HiSegX, with 150 bp, paired-end reads, resulting in the sequencing of 448,360,724 total read pairs after cleaning and processing (SI Appendix Tables S1 and S2). Quality control was performed with FastQC and trimming with Trimmomatic (parameter settings of ILLUMINACLIP: TruSeq3-PE-2.fa:2:30:10, LEADING:5, TRAILING:5, SLIDINGWINDOW: 4:15, MINLEN:35, HEADCROP:15). De novo transcript assembly was performed with Trinity-v2.6.6 (22, 23), using the default settings of >95% identity and a minimum assembled contig length of 200 nucleotides, resulting in the assembly of 915,085 transcripts that clustered as 536,644 genes (SI Appendix Table S3). RSEM, which uses bowtie2 for alignment, was used to quantify the expression of genes and transcripts (48), and edgeR for the identification of DEGs (dispersion setting 0.1) (49) (SI Appendix Fig. S2, Dataset S1). Expression levels are reported as centered log2 (fpkm+1) values as this enables analysis according to relative expression across the different samples. For annotation, TransDecoder v5.5.0 (http://transdecoder.sf.net) was used to identify candidate coding regions and generate peptide sequence files of at least 100 amino acids from the open reading frames. Putative annotations were assigned using Trinotate and The At Information Resource 10 protein database was used for BLASTP v2.9.0+ search; all annotated genes with the top blastP homology were used for further analysis (parameters: -e-value: 1e-05 -outfmt 6) (SI Appendix Fig. S3, Datasets S2 and S3).

Metabolite analysis

Floral tissues from the 2022 titan arum bloom of Morphy and leaf tissue from Maudine x Woody #3 (SI Appendix Fig. S5) were used for amino acid and putrescine extraction and detection. Floral tissue samples were collected from the appendix, the spathe margin, and the spathe base at day 0 (D-day) of the bloom prior to the peak of thermogenesis (17:00 h) and after the peak of thermogenesis (23:00 h) and flash-frozen in liquid nitrogen. Tissue was freezedried and then pulverized using a mixer mill (Retsch Mill, MM400), and free and protein-bound amino acids were extracted, detected, and quantified by LC-MS/MS as previously described (50, 51) (Dataset S5). Putrescine was extracted, derivatized, and detected using GC-MS (Agilent 8890N GC coupled to a 5977C mass selective detector) like previously described (52). Putrescine was quantified based on comparison to an authentic putrescine standard (Sigma) curve and resolved on a 60 m VF-5 column (SI Appendix Fig. S6). ANOVA-based statistical analysis was performed with the online calculator (https://astatsa.com/).

Acknowledgments

The authors thank K. Arumuganathan of the Benaroya Research Institute at Virginia Mason, Flow Cytometry and Imaging Core Laboratory, for flow cytometry analysis; Nathan Giffard and Celia Chen (Dartmouth College) for assistance in sample freezedrying; and Robert Raguso (Cornell University) and Georg Jander (Boyce Thompson Institute) for helpful discussions.

Supplementary Material

Supplementary material is available at PNAS Nexus online.

Funding

This work was supported by the National Science Foundation grants MCB-1517032, IOS-1856513, and IOS-2425472 to G.E.S.

Author Contributions

G.E.S. was involved in conception of project and supervision. A.Z., B.J.A., S.N.S., K.G., C.A.S., T.D.B., D.O., K.D., R.A., and G.E.S. were involved in methodology and writing—review and editing. A.Z., B.J.A., S.N.S., C.A.S., T.D.B., D.O., K.D., and G.E.S. were involved in investigation. A.Z., C.A.S., and G.E.S. were involved in visualization. G.E.S., S.N.S., and C.A.S. were involved in project administration. A.Z. and G.E.S. were involved in writing—original draft.

Data Availability

RNA-seq data have been deposited at Sequence Read Archive (Bioproject no. PRJNA989517 and Biosample no. SUB13583247). Trinity-assembled transcripts have been deposited at Digital Commons (https://digitalcommons. dartmouth.edu/facoa/4338). All data are available in the main text or the supplementary materials.

References

- Claudel C, Loiseau O, Silvestro D, Lev-Yadun S, Antonelli A. 2023. Patterns and drivers of heat production in the plant genus Amorphophallus. Plant J. 115:874-894.
- Barthlott W, Szarzynski J, Vlek P, Lobin W, Korotkova N. 2009. A torch in the rain forest: thermogenesis of the Titan arum (Amorphophallus titanum). Plant Biol (Stuttg). 11:499-505.
- A. M. Bertholet, Y. Kirichok. 2022. Mitochondrial H(+) leak and thermogenesis. Annu Rev Physiol. 84:381-407.
- McDonald AE. 2023. Unique opportunities for future research on the alternative oxidase of plants. Plant Physiol. 191:2084-2092.
- Moller IM. 2001. Plant mitochondria and oxidative stress: electron transport, NADPH turnover, and metabolism of reactive oxygen species. Annu Rev Plant Physiol Plant Mol Biol. 52:561-591.
- Cannon B, Nedergaard J. 2004. Brown adipose tissue: function and physiological significance. Physiol Rev. 84:277-359.
- Raskin I, Ehmann A, Melander WR, Meeuse BJ. 1987. Salicylic acid: a natural inducer of heat production in arum lilies. Science. 237:1601-1602.
- Raskin I, Turner IM, Melander WR. 1989. Regulation of heat production in the inflorescences of an Arum lily by endogenous salicylic acid. Proc Natl Acad Sci U S A. 86:2214-2218.
- Rhoads DM, McIntosh L. 1992. Salicylic acid regulation of respiration in higher plants: alternative oxidase expression. Plant Cell.
- 10 Onda Y, et al. 2015. Transcriptome analysis of thermogenic Arum concinnatum reveals the molecular components of floral scent production. Sci Rep. 5:8753.
- 11 Dudareva N, Klempien A, Muhlemann JK, Kaplan I. 2013. Biosynthesis, function and metabolic engineering of plant volatile organic compounds. New Phytol. 198:16-32.
- 12 Muhlemann JK, Klempien A, Dudareva N. 2014. Floral volatiles: from biosynthesis to function. Plant Cell Environ. 37:1936-1949.
- 13 Kite GC, Hetterschieid WLA. 1997. Inflorescence odours of Amorphophallus and Pseudodracontium (Araceae). Phytochemistry. 46:71-75.

- 14 Kite GC, Hetterscheid WLA. 2017. Phylogenetic trends in the evolution of inflorescence odours in Amorphophallus. Phytochemistry. 142:126-142.
- 15 Shirasu M, et al. 2010. Chemical identity of a rotting animal-like odor emitted from the inflorescence of the titan arum (Amorphophallus titanum). Biosci Biotechnol Biochem. 74:2550–2554.
- 16 Kang L, Kaur J, Winkeler K, Kubiak D, Hill JE. 2023. How the volatile organic compounds emitted by corpse plant change through flowering. Sci Rep. 13:372.
- 17 Liu D, et al. 2023. An analysis of volatile vompounds and study of release regularity in the flower of Amorphophallus titanum in four periods. Horticulturae. 9:487.
- 18 Szenteczki MA, et al. 2022. Transcriptomic analysis of deceptively pollinated Arum maculatum (Araceae) reveals association between terpene synthase expression in floral trap chamber and species-specific pollinator attraction. G3 (Bethesda). 12:jkac175.
- 19 Ito-Inaba Y, et al. 2012. The gene expression landscape of thermogenic skunk cabbage suggests critical roles for mitochondrial and vacuolar metabolic pathways in the regulation of thermogenesis. Plant Cell Environ. 35:554-566.
- Dolezel J, Bartos J. 2005. Plant DNA flow cytometry and estimation of nuclear genome size. Ann Bot. 95:99-110.
- 21 Bainard JD, Bainard LD, Henry TA, Fazekas AJ, Newmaster SG. 2012. A multivariate analysis of variation in genome size and endoreduplication in angiosperms reveals strong phylogenetic signal and association with phenotypic traits. New Phytol. 196: 1240-1250.
- 22 Grabherr MG, et al. 2011. Full-length transcriptome assembly from RNA-Seq data without a reference genome. Nat Biotechnol. 29:644-652.
- 23 Haas BJ, et al. 2013. De novo transcript sequence reconstruction from RNA-seq using the Trinity platform for reference generation and analysis. Nat Protoc. 8:1494-1512.
- 24 Lobin W, Neumann M, Radscheit M, Barthlott W. 2007. The cultivation of titan arum (Amorphophallus titanum): a flagship species for botanic gardens. Sibbaldia Int J Botanic Garden Horticulture. 5: 69-86.
- 25 Lytle CM, Smith BN, Hopkin MS, Hansen LD, Criddle RS. 2000. Oxygen-dependence of metabolic heat production in the appendix tissue of the voodoo lily (Sauromatum guttatum Schott). Thermochim Acta. 349:135-140.
- 26 Slewinski TL. 2011. Diverse functional roles of monosaccharide transporters and their homologs in vascular plants: a physiological perspective. Mol Plant. 4:641-662.
- 27 Chen LQ, Cheung LS, Feng L, Tanner W, Frommer WB. 2015. Transport of sugars. Annu Rev Biochem. 84:865-894.
- 28 Skubatz H, Kunkel HH, Meeuse BJD. 1993. Ultrastructural changes in the appendix of the Sauromatum guttatum inflorescence during anthesis. Sex Plant Reprod. 6:153-170.
- 29 Ito K, Seymour RS. 2005. Expression of uncoupling protein and alternative oxidase depends on lipid or carbohydrate substrates in thermogenic plants. Biol Lett. 1:427-430.
- 30 Burton JD. 2023. Approach to the autopsy examamination of an adult decomposing body. Diagn Histopathology. 29:340-346.
- 31 Ciesla J, et al. 2023. The smell of death. State-of-the-art and future research directions. Front Microbiol. 14:1260869.
- 32 Yao X, Nie J, Bai R, Sui X. 2020. Amino acid transporters in plants: identification and function. Plants (Basel). 9:972.
- 33 Rébeillé F, et al. 2006. Methionine catabolism in Arabidopsis cells is initiated by a gamma-cleavage process and leads to S-methylcysteine and isoleucine syntheses. Proc Natl Acad Sci USA. 103:15687-15692.

- 34 Xu Y-H, Jia K-Z, Tang Y-J. 2018. Regulatory networks governing methionine catabolism into volatile organic sulfur-containing compounds in Clonostachys rosea. Appl Environ Microbiol. 84: e01840-18.
- 35 Hazelwood LA, Daran JM, van Maris AJ, Pronk JT, Dickinson JR. 2008. The Ehrlich pathway for fusel alcohol production: a century of research on Saccharomyces cerevisiae metabolism. Appl Environ Microbiol. 74:2259–2266.
- 36 Chin H-W, Lindsay RC. 1994. Mechanisms of formation of volatile sulfur compounds following the action of cysteine sulfoxide lyases. J Agric Food Chem. 42:1529–1536.
- 37 Rabinkov A, Zhu XZ, Grafi G, Galili G, Mirelman D. 1994. Alliin lyase (Alliinase) from garlic (Allium sativum). Biochemical characterization and cDNA cloning. Appl Biochem Biotechnol. 48:149–171.
- 38 Sun X, et al. 2020. A chromosome-level genome assembly of garlic (Allium sativum) provides insights into genome evolution and allicin biosynthesis. Mol Plant. 13:1328–1339.
- 39 Neuhierl B, Thanbichler M, Lottspeich F, Bock A. 1999. A family of S-methylmethionine-dependent thiol/selenol methyltransferases. Role in selenium tolerance and evolutionary relation. *J Biol Chem.* 274:5407–5414.
- 40 Lyi SM, et al. 2005. Molecular and biochemical characterization of the selenocysteine Se-methyltransferase gene and Se-methylselenocysteine synthesis in broccoli. Plant Physiol. 138:409–420.
- 41 Winter G, Todd CD, Trovato M, Forlani G, Funck D. 2015. Physiological implications of arginine metabolism in plants. Front Plant Sci. 6:534.
- 42 Plotka-Wasylka JM, Morrison C, Biziuk M, Namiesnik J. 2015. Chemical derivatization processes applied to amine determination

- in samples of different matrix composition. Chem Rev. 115: 4693–4718.
- 43 Raman V, Tabanca N, Demirci B, Khan IA. 2017. Studies on the floral anatomy and scent chemistry of titan arum (*Amorphophallus titanum*, Araceae). Turkish J Botany. 41:63–74.
- 44 Arumuganathan K, Earle E. 1991. Estimation of nuclear DNA content of plants by cell-flow cytometry. Plant Mol Biol Rep. 9:229–233.
- 45 Tsai CJ, Cseke LJ, Harding SA. 2011. Isolation and purification of RNA. In: Cseke LK, Kirakosyan A, Kaufman PB, Westfall MV, editors. Handbook of molecular and cellular methods in biology and medicine. CRC Press. p. 167–186.
- 46 Wang L, et al. 2011. A low-cost library construction protocol and data analysis pipeline for Illumina-based strand-specific multiplex RNA-seq. PLoS One. 6:e26426.
- 47 Kumar R, et al. 2012. A high-throughput method for Illumina RNA-Seq library preparation. Front Plant Sci. 3:202.
- 48 Li B, Dewey CN. 2011. RSEM: accurate transcript quantification from RNA-Seq data with or without a reference genome. BMC Bioinformatics. 12:323.
- 49 Robinson MD, McCarthy DJ, Smyth GK. 2010. Edger: a bioconductor package for differential expression analysis of digital gene expression data. Bioinformatics. 26:139–140.
- 50 Yobi A, et al. 2020. The complex response of free and bound amino acids to water stress during the seed setting stage in Arabidopsis. Plant J. 102:838–855.
- 51 Angelovici R, et al. 2017. Network-guided GWAS improves identification of genes affecting free amino acids. Plant Physiol. 173: 872–886.
- 52 Schenck CA, et al. 2020. Role of cytosolic, tyrosine-insensitive prephenate dehydrogenase in Medicago truncatula. Plant Direct. 4: e00218.



Supporting Information for

Molecular basis for thermogenesis and volatile production in the titan arum

Alveena Zulfiqar^{1,2,#}, Beenish Azhar^{1,2,#}, Samina N. Shakeel^{1,2}, William Thives Santos³, Theresa D. Barry¹, Dana Ozimek¹, Kim DeLong¹, Ruthie Angelovici⁴, Kathleen M. Greenham^{1,5}, Craig A. Schenck³, G. Eric Schaller^{1*}

G. Eric Schaller Email: george.e.schaller@dartmouth.edu

This PDF file includes:

Figures S1 to S6 Tables S1 to S3 Legends for Datasets S1 to S5

Other supporting materials for this manuscript include the following:

Datasets S1 to S5

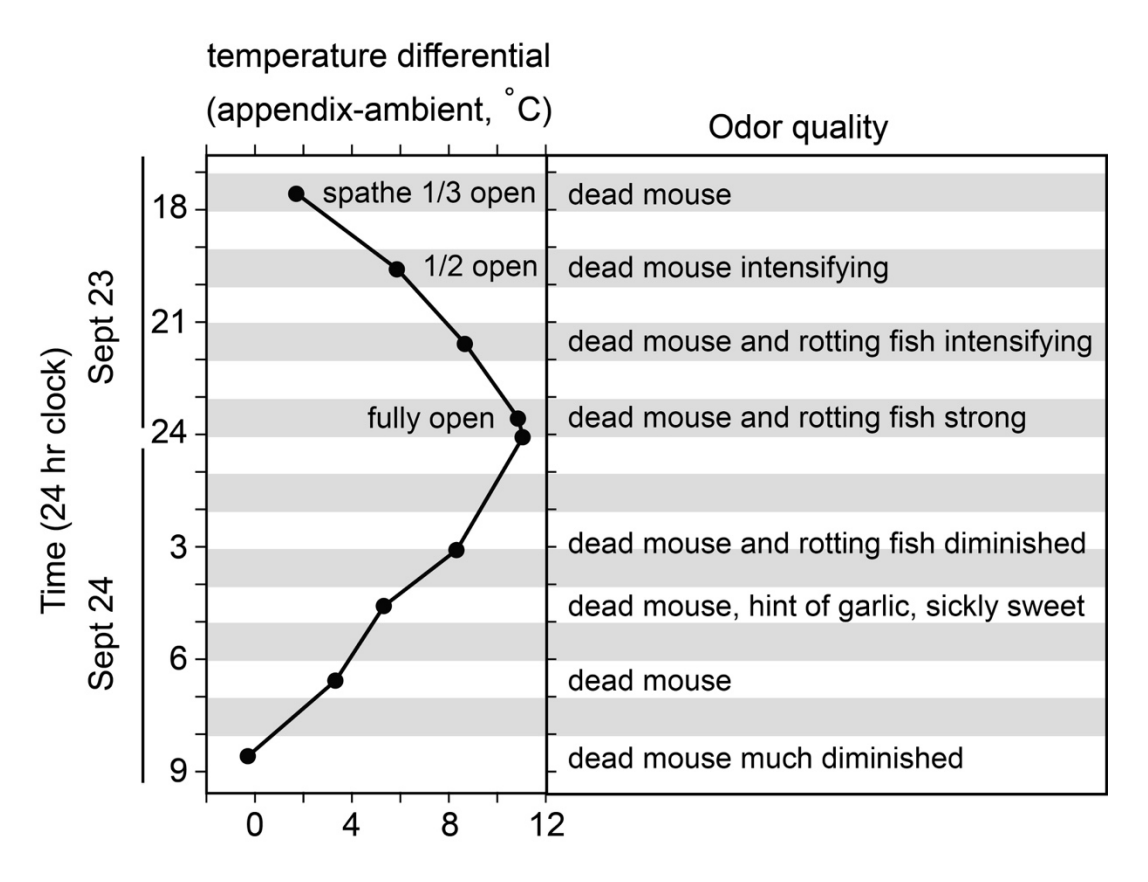


Figure S1. Temperature differential and odor quality of the 2016 bloom of the titan arum 'Morphy'

The time course record shows the difference between the surface temperature of the appendix and the ambient temperature on D-day when the spathe opened. The odor quality was noted by co-author Theresa Barry at the same time as when the temperature readings of the titan arum were taken. See also Fig. 1.

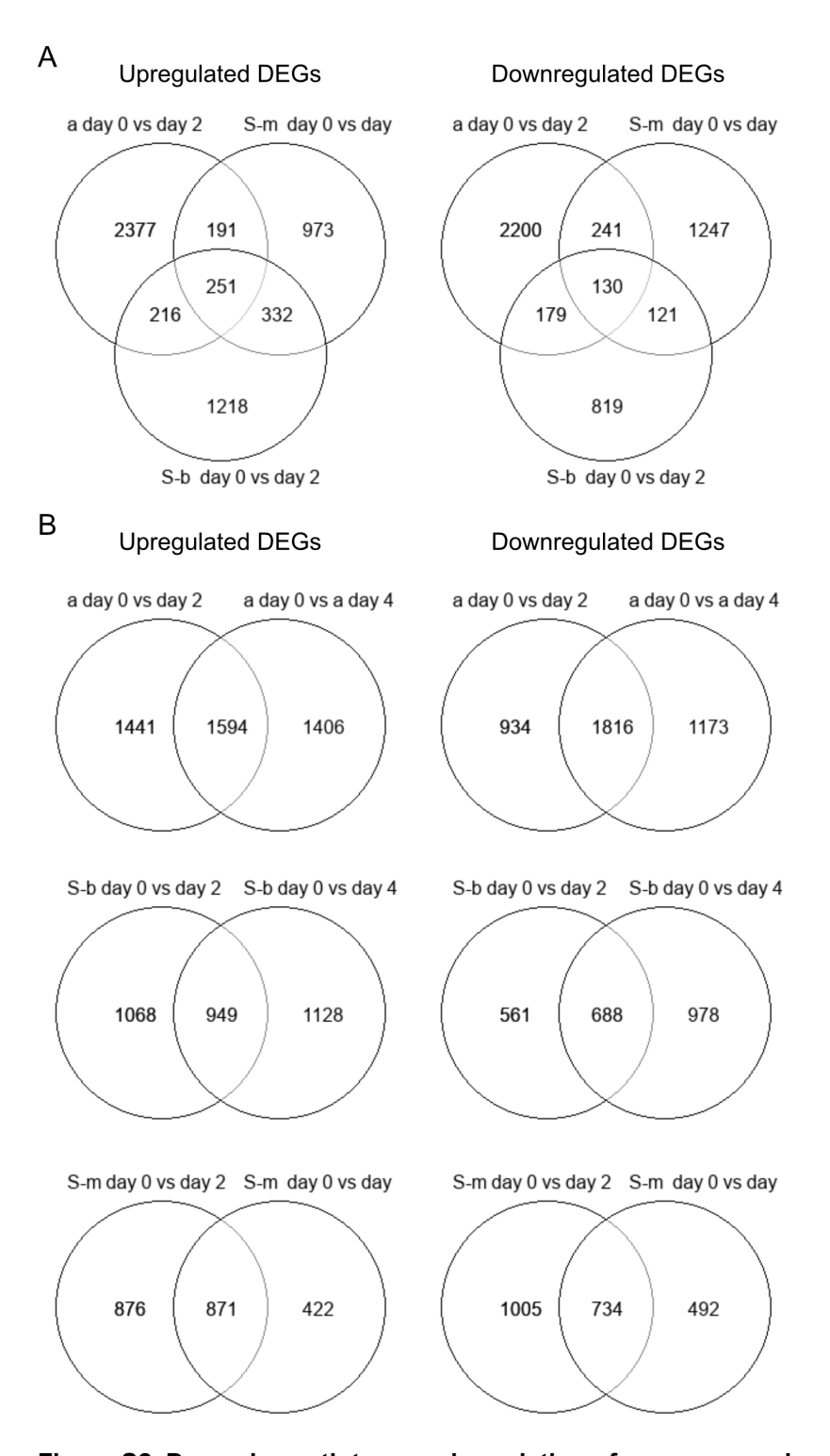


Figure S2. Dynamic spatiotemporal regulation of gene expression

Differentially expressed genes (DEGs; 4-fold difference in expression; p < 0.05) from the appendix (a), spathe base (s-b), and spathe margin (s-m) are compared. (A) Comparison of DEGs identified between days 0 and 2 for the appendix, spathe base, and spathe margin. (B) Comparison of DEGs identified between days 0 and 2, and days 0 and 4 for each of the tissues. See also Fig. 1.

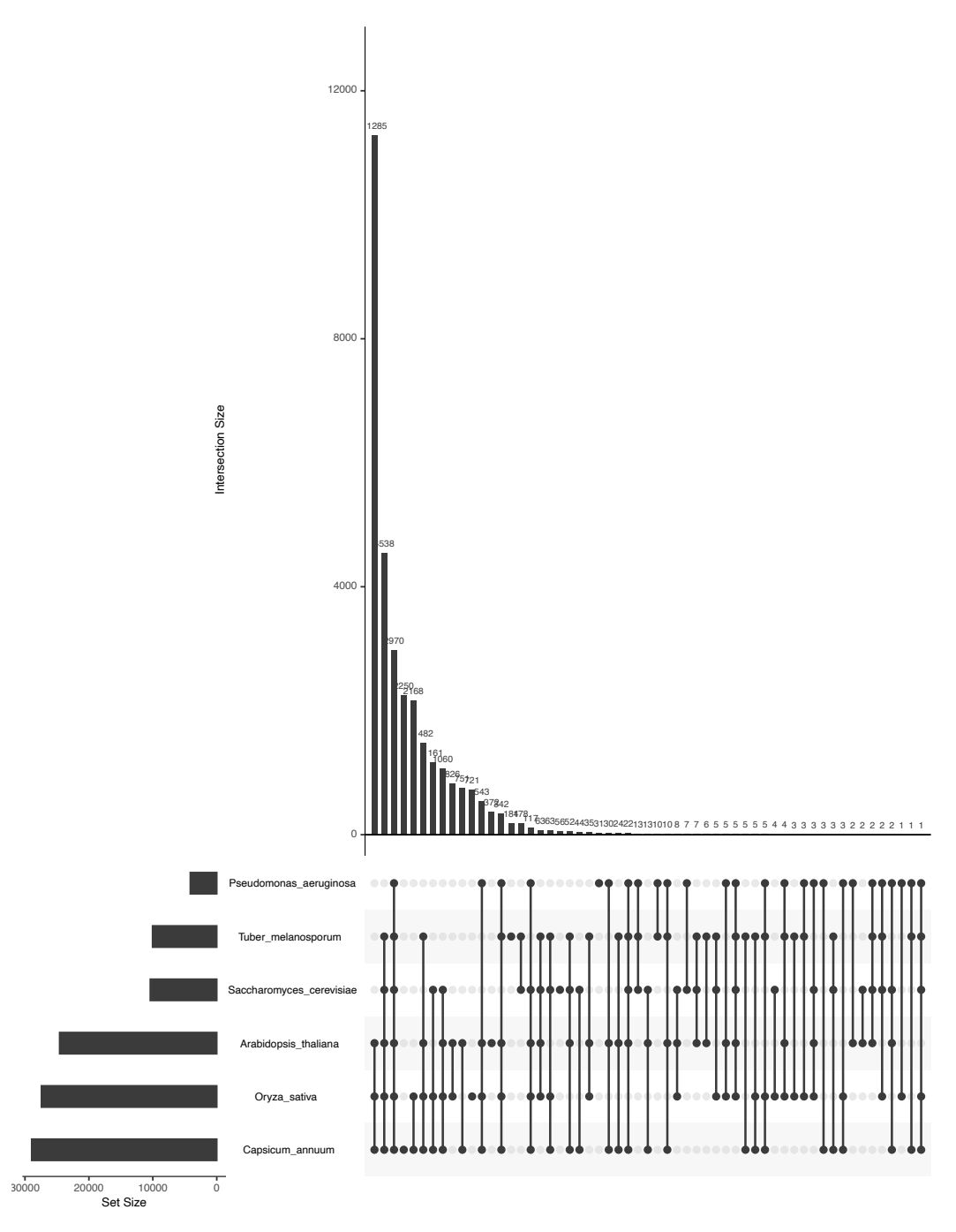


Figure S3. Intersection of Trinity genes of the monocotyledonous titan arum with plant, fungi, and bacterial genomes

Intersections are shown for the monocot *Oryza sativa* (rice), the dicots *Arabidopsis thaliana* and *Capsicum annuum* (pepper), the fungi *Saccharomyces cerevisiae* and *Tuber melanosporum* (truffle), and the bacterium *Pseudomonas aeruginosa*.

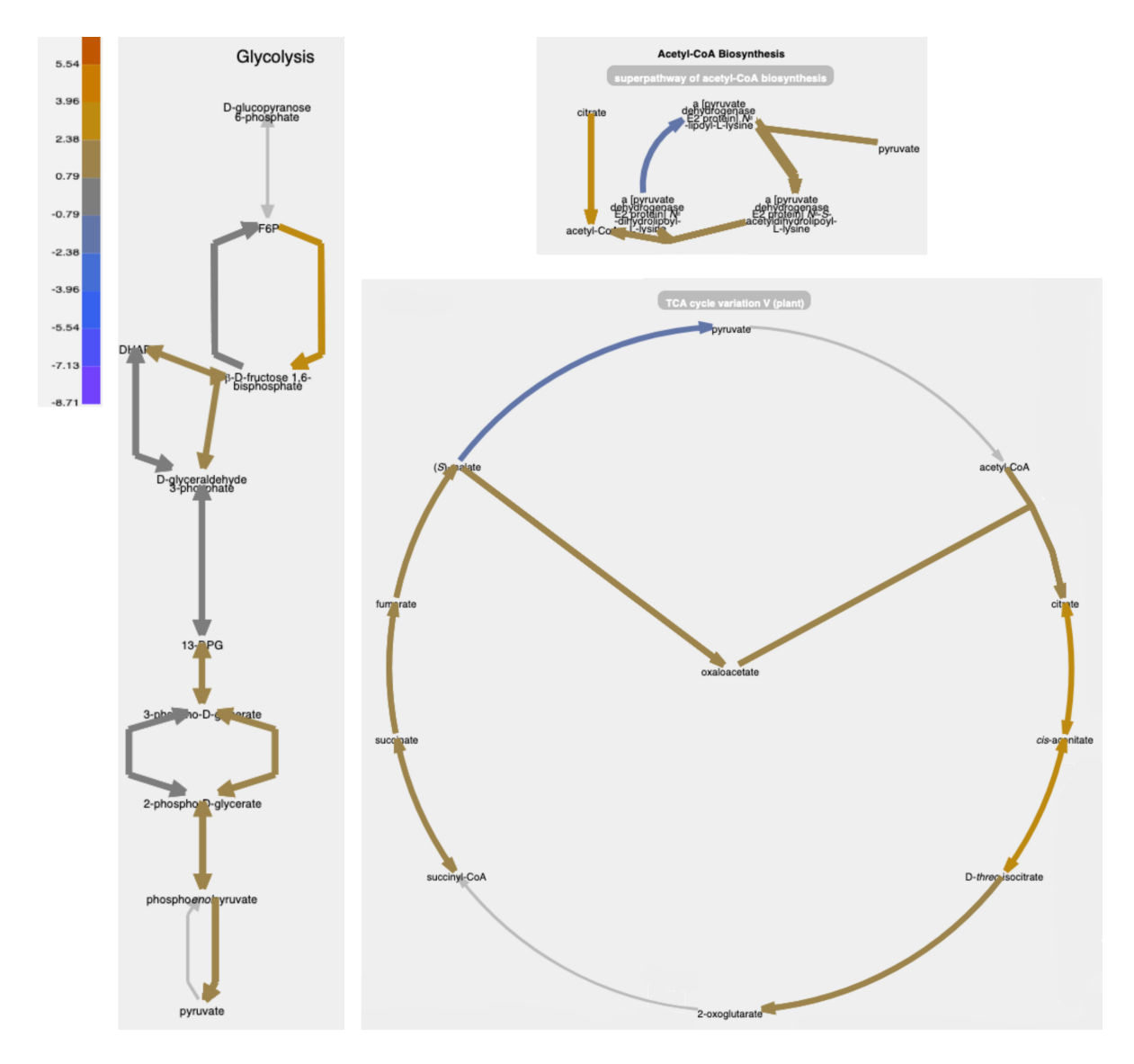


Figure S4. Identification and comparative expression between days 0 and 4 of the appendix for genes involved in glucose metabolism

Genes are overlaid on the enzymatically catalyzed steps of glycolysis, the conversion between pyruvate and acetyl-CoA, and the TCA cycle. Differential expression between days 0 and 4 is indicated by color. See also Fig. 2.

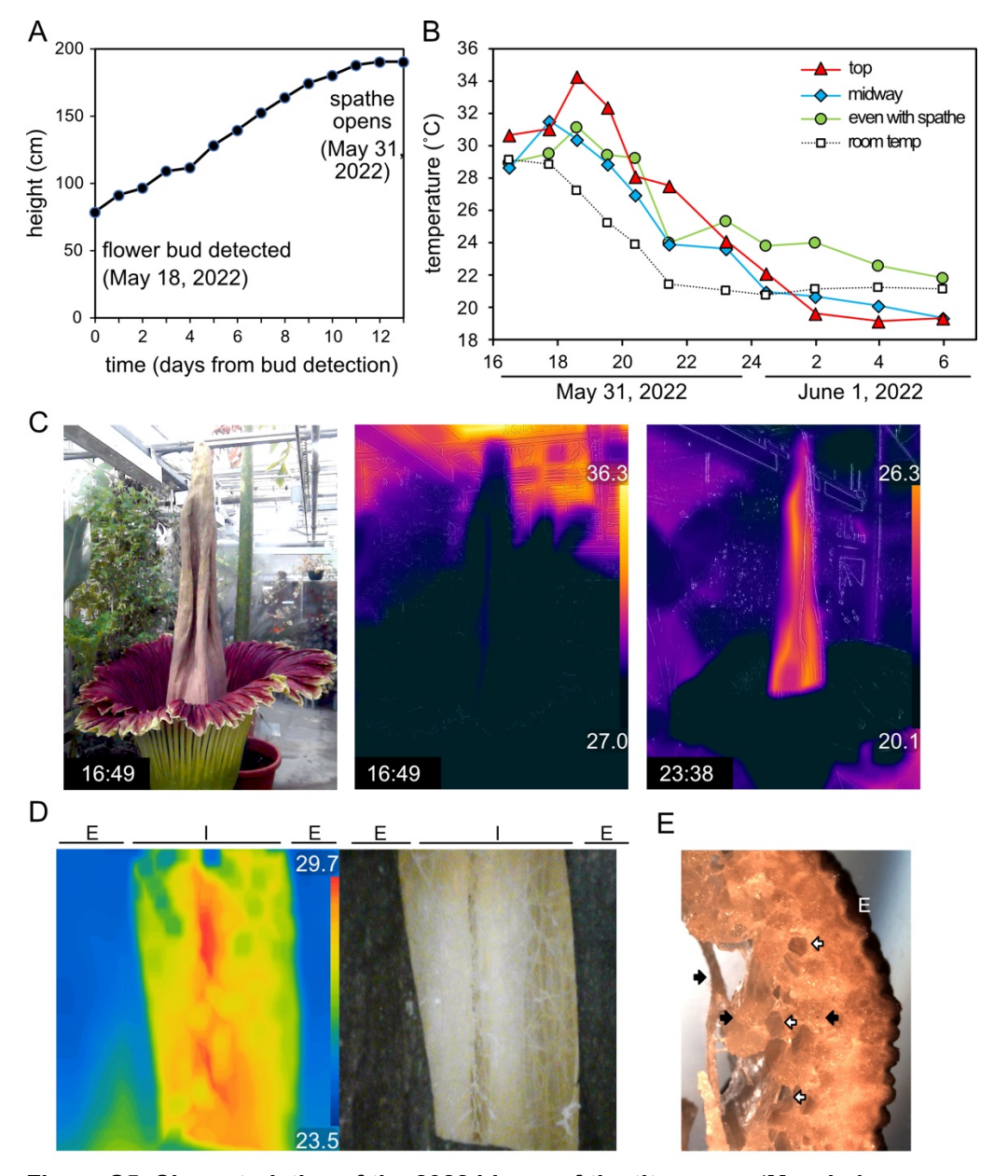


Figure S5. Characteristics of the 2022 bloom of the titan arum 'Morphy'

- **(A)** Growth leading up to spathe opening. Height was measured from point of soil emergence to tip of the appendix.
- **(B)** Thermogenic phase of the inflorescence following opening of the spathe on May 31, 2022. The surface temperature of the appendix was measured at three locations (top, midway, and even with the spathe) over a period of 14 hr and compared to ambient air temperature.
- **(C)** Thermal imaging of Morphy at the times (lower left) of tissue collection for amino-acid analysis, prior to and after the peak of thermogenesis. Temperature scales are set to reveal thermogenesis above the ambient air temperature.
- **(D)** Heightened thermogenesis from interior (I) cells as compared to the exterior (E) epidermal cells of the appendix, as determined by cutting a window into the hollow appendix.
- **(E)** Cross section of appendix (E = epidermis side), with examples of aerenchyma (white arrows) and vasculature containing xylemic canals (black arrows) indicated.

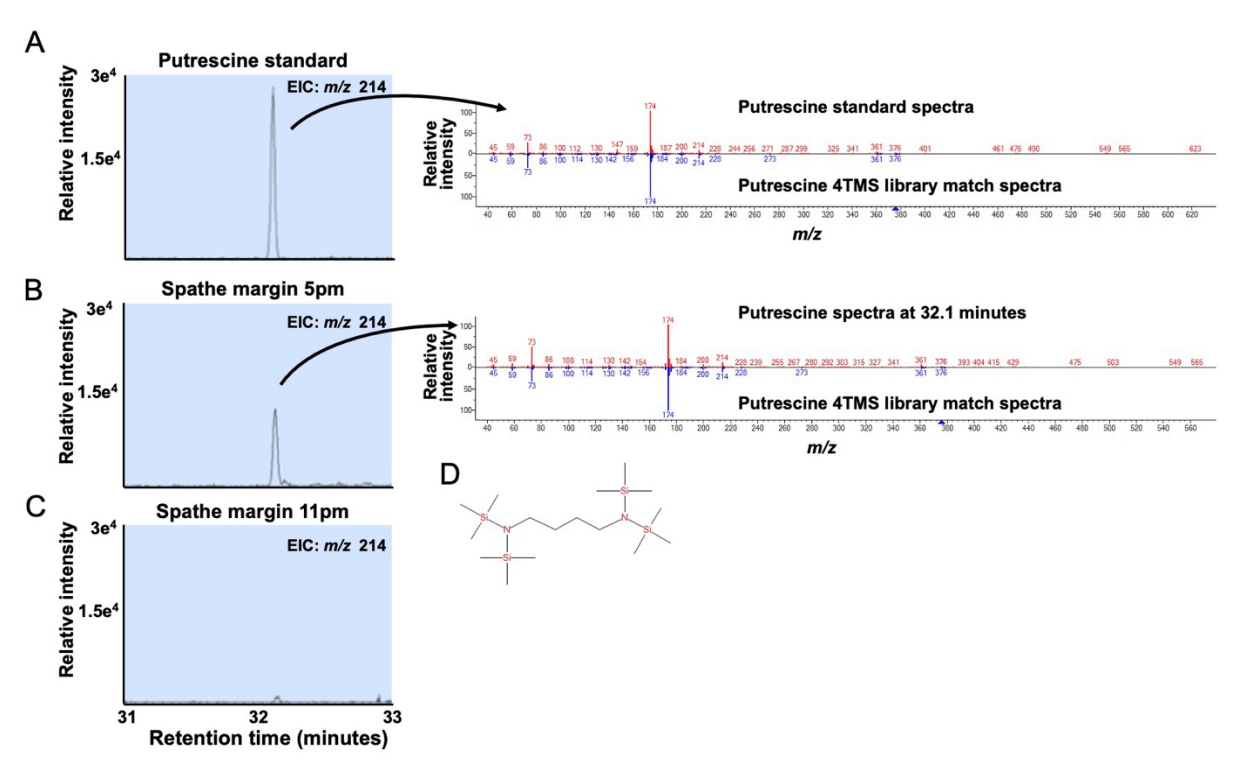


Figure S6. Putrescine detection from Titan arum tissue

Titan arum metabolites were derivatized with trimethylsilyl (TMS) reagent and detected using gas chromatography-mass spectrometry (GC-MS).

- (A) An authentic putrescine standard had a near identical mass spectra to a 4TMS putrescine derivative in the NIST library. An extracted ion chromatogram (EIC) is shown for a distinct fragment ion 214 m/z.
- **(B)** Putrescine was detected in the spathe margin at 5pm and had a mass spectra nearly identical to 4TMS spectra in the NIST library and similar retention time to the authentic putrescine standard.
- (C) Putrescine levels were substantially reduced in the spathe margin at 11 pm.
- **(D)** Structure of 4TMS putrescine derivative.

Table S1. RNA-seq read data for the titan arum

	APPENDIX -D0	SPATHEB- D0	SPATHEM- D0	APPENDIX -D2	SPATHEB- D2	SPATHEM- D2	APPENDIX -D4	SPATHEB- D4	SPATHEM- D4	LEAF1	LEAF2	TOTAL
Raw read pairs	40,126,818	34,825,528	39,608,082	41,266,076	40,002,090	40,401,438	42,741,465	40,196,862	42,497,214	52,203,951	48,920,098	462,789,622
Raw length	150	150	150	150	150	150	150	150	150	150	150	
Clean and processed read pairs	38,864,349	33,729,872	38,385,506	39,947,968	38,720,054	39,148,277	41,374,795	39,002,896	41,128,736	50,636,614	47,421,657	448,360,724
Processed read length	20-135	20-135	20-135	20-135	20-135	20-135	20-135	20-135	20-135	20-135	20-135	

Table S2: RNA-seq data deposited with the Sequence Read Archive (SRA)

accession	study	bioproject_accession	biosample_accession	sample_name	library_ID
SRR25083333	SRP446746	PRJNA989517	SAMN36093314	Appendix Day 0	a_day0
SRR25083332	SRP446746	PRJNA989517	SAMN36093315	Spathe Base Day 0	s_b_day0
SRR25083330	SRP446746	PRJNA989517	SAMN36093316	Spathe Margin Day 0	s_m_day0
SRR25083329	SRP446746	PRJNA989517	SAMN36093317	Appendix Day 2	a_day2
SRR25083328	SRP446746	PRJNA989517	SAMN36093318	Spathe Base Day 2	s_b_day2
SRR25083327	SRP446746	PRJNA989517	SAMN36093319	Spathe Margin Day 2	s_m_day2
SRR25083326	SRP446746	PRJNA989517	SAMN36093320	Appendix Day 4	a_day4
SRR25083325	SRP446746	PRJNA989517	SAMN36093321	Spathe Base Day 4	s_b_day4
SRR25083324	SRP446746	PRJNA989517	SAMN36093322	Spathe Margin Day 4	s_m_day4
SRR25083323	SRP446746	PRJNA989517	SAMN36093323	Leaf 1	11
SRR25083331	SRP446746	PRJNA989517	SAMN36093324	Leaf 2	12

Table S3. Characteristics of Trinity gene assembly for the titan arum

	All transcript contigs ^a	Longest isoform per 'gene'b
Median contig length	356	321
Average contig length	646.87	496.24
Total assembled bases	591,941,432	266,305,938

abased on 915,085 total trinity transcripts based on 536,644 total trinity 'genes'

Dataset S1. (separate file)

DEGs that exhibited at least 2-fold or 4-fold expression change in appendix day 0 compared to appendix day 2 (p <0.05) (see Figure 1D).

Dataset S2. (separate file)

Annotation of Trinity genes for titan arum based on six genomes from plants, fungi, and bacteria. (see Figure S2).

Dataset S3. (separate file)

Arabidopsis annotation of Trinity genes for titan arum (p < 0.05). (see Figures 2, 3, and 4).

Dataset S4. (separate file)

Trinity genes, Arabidopsis annotation, and gene expression information related to cellular respiration, sugar and amino acid transport, thermogenesis, sulfur transport and metabolism, arginine metabolism, and SA metabolism. (see Figures 2, 3, and 4).

Dataset S5. (separate file)

Amino acid analysis. (see Figures 3 and 4).